RSC Advances

PAPER

View Article Online
View Journal | View Issue

Cite this: *RSC Adv.*, 2025, **15**, 22699

Study on the influence of different factors on the direct treatment of high turbidity water by microfiltration processes

Xiaosan Song, *[ab] Ping Li,[ab] Qingchao Shen,*[ab] Wenxuan Wei[ab] and Hairong Yan[ab]

Currently, traditional high turbidity water treatment technologies (coagulation–sedimentation–filtration) face issues such as non-compliant effluent quality, sediment compaction, and poor sludge discharge. Meanwhile, membrane filtration technology suffers from severe membrane fouling in high turbidity water treatment. Therefore, the development of green and low-carbon high turbidity water treatment technologies is urgently needed. This study employs microfiltration to directly filter high turbidity water, investigating turbidity, filtration methods, and transmembrane pressure difference to elucidate the mechanisms of mitigating membrane fouling in high turbidity water treatment. The results indicate that both excessively high and low influent turbidity are detrimental to high turbidity water treatment. Low turbidity fails to effectively protect the membrane, exacerbating membrane fouling, while high turbidity leads to excessive cake layer thickness, reducing membrane flux. Therefore, the optimal treatment turbidity must be determined based on the specifications of the experimental setup. In this study, the optimal treatment turbidity is 900 NTU. Under constant pressure conditions, cross-flow filtration effectively controls the thickness of the filter cake layer, mitigates membrane fouling, and maintains a high membrane flux. When the influent turbidity is 900 NTU, the membrane flux recovery rate and filtration flux are 80.14% and 0.9077 m h^{-1}, respectively, with irreversible membrane fouling being only 0.97 × 10^{10} m^{-1}. At a constant influent turbidity, higher transmembrane pressure difference increases the filtration flux but exacerbates membrane fouling. When the pressure increases from 6.67 kPa to 33.33 kPa, irreversible membrane fouling increases by 27.97%, while the filtration flux increases by 116.91%. At a pressure of 13.33 kPa, although the filtration flux is 56.83% of that at 33.33 kPa, the irreversible membrane fouling is only 62.25%. Therefore, this study identifies 13.33 kPa as the optimal transmembrane pressure difference. The Hermia model revealed that transmembrane pressure difference was the primary factor aggravating membrane fouling. Finally, through dosing $FeCl_3$ as a coagulant for cake layer regulation, the cake layer structure formed at 15 mg per L dosage showed optimal pollutant interception and removal efficiency: humic acid (HA) removal efficiency reached 75.86% in actual water sources with 79.06% flux recovery rate; simulated feed water achieved 77.44% HA removal with 84.31% flux recovery rate. This study aims to provide reference for microfiltration processes in direct treatment of high-turbidity water.

Received 14th March 2025
Accepted 17th June 2025

DOI: 10.1039/d5ra01817j

rsc.li/rsc-advances

1 Introduction

China is a country with water scarcity, ranking sixth in the world in terms of water reserves, but its per capita water availability is low, making it one of the most water-scarce countries globally.[1,2] Currently, half of China's regions face water scarcity or severe water shortages, particularly in northern China, where water resources account for only 17% of the national total, highlighting the severity of the water shortage issue.[3] The Yellow River supplies water to more than 50 cities, serving as the primary water source for urban areas within its basin. At the same time, the Yellow River is a typical high-turbidity river, with the highest sediment concentration in the world, placing significant pressure on water treatment plants along its banks to handle high-turbidity water year-round.[4] Therefore, researching and developing effective high-turbidity water treatment processes is of great significance for ensuring sustainable social and economic development.

Currently, conventional water treatment technologies dominated by coagulation are the most widely used for high-turbidity water treatment, primarily achieved by adjusting coagulant dosage, developing new coagulants, and optimizing

[a]*Key Laboratory of Yellow River Water Environment in Gansu Province, Lanzhou Jiaotong University, Lanzhou 730070, China. E-mail: songxs@mail.lzjtu.cn; 13964762817@163.com*

[b]*Engineering Research Center for Comprehensive Utilization of Water Resources in Cold and Arid Regions, Ministry of Education, Lanzhou 730070, China*

coagulation conditions.[5,6] Xu *et al.*[7] enhanced the floc structure formed during coagulation by preparing an inorganic flocculant, polysilicate iron, and subsequently achieved the treatment of high-turbidity tailings water through sedimentation and filtration processes. Hessam *et al.*[8] also focused on coagulants, using pomegranate powder as a natural coagulant, and achieved the treatment of high-turbidity industrial wastewater with a turbidity of 1150 NTU through coagulation, sedimentation, and filtration processes. However, in high-turbidity water treatment, enhanced coagulation processes often require large amounts of chemicals to achieve purification, leading to issues such as chemical waste and residual contamination.[9]

Membrane filtration technology, as one of the most advanced water purification technologies today, offers advantages such as efficient pollutant interception, simple operation, excellent permeability, and ease of operational management.[10] Ye Chunsong *et al.*[11] used PVDF ultrafiltration membranes to directly treat high-turbidity seawater (60–3000 NTU). The experiments showed that the effluent turbidity was reduced to 0.11 NTU, with a colloidal silica removal rate of up to 89%. Notably, the transmembrane pressure difference of the membrane module remained below 6.0×10^4 Pa, only 28.57% of the maximum operating pressure. This indicates that ultrafiltration membranes exhibit strong adaptability and effectiveness in treating high-turbidity water. In the study of post-disaster high-turbidity surface water, Li Yonghong[12] found that membrane filtration technology could consistently control the effluent turbidity below 0.2 NTU. After hydraulic backwashing, pollutants on the membrane surface were almost completely removed, and the backwash flux recovery rate reached 96–99%. Therefore, membrane filtration technology not only achieves high removal rates but also exhibits strong tolerance to turbidity when treating high-turbidity water, making it feasible to directly apply membrane filtration technology for high-turbidity water treatment.

Membrane fouling is currently the primary limitation of membrane filtration technology in high-turbidity water applications. Jin *et al.*[13,14] found that when using membrane technology to directly treat municipal wastewater, the membrane's permeability sharply decreased after only 5–7 hours of filtration, necessitating the addition and use of coagulants/air scouring/backwashing methods to extend filtration time. Similarly, Kimura *et al.*[15] found that when filtering municipal wastewater with membranes, the operating transmembrane pressure (approximately 45 kPa) increased sharply within the first 5 minutes of filtration, requiring the simultaneous use of membrane vibration, mechanical stirring, and periodic chemical backwashing to control membrane fouling and prevent severe pollution issues during filtration. Therefore, although direct ultrafiltration technology experiences membrane fouling when treating high-turbidity water, it can be alleviated through methods such as chemical backwashing, aeration, and membrane rotation.

Sanchis-Perucho *et al.*[16] found in their study on the feasibility of directly treating urban wastewater with membrane filtration technology that increasing the influent solid particle concentration and size promotes the formation of a reversible cake layer on the membrane surface, reduces interactions between the membrane and highly contaminating substances, and decreases the proportion of irreversible membrane fouling. Additionally, the reversible cake layer formed by larger influent particle sizes exhibits higher porosity, ensuring a certain level of permeability flux. Kuberkar *et al.*[17] found that during ultrafiltration membrane filtration, larger particles deposit on the membrane surface and gradually form a cake-like structure. This structure exhibits a specific spatial arrangement, maintains water flux while effectively intercepting smaller particles, mitigates membrane fouling, and functions similarly to a deep filter bed. Therefore, in high-turbidity water treatment, rapidly forming a filter cake layer of specific thickness on the membrane surface can effectively alleviate membrane fouling, though research in this area remains limited.

This study employed microfiltration for direct treatment of high-turbidity water, investigating membrane filtration performance through four aspects: turbidity, filtration mode, transmembrane pressure difference, and $FeCl_3$ coagulant dosage. Optimal treatment parameters including turbidity, filtration mode, transmembrane pressure difference, and $FeCl_3$ dosage were determined through flux recovery rate and membrane fouling resistance analysis. The membrane fouling control mechanisms of direct microfiltration in high-turbidity water treatment were elucidated. Cake layer porosity analysis and Hermia modeling revealed the impacts of different operational conditions on membrane blocking types. Finally, pollutant removal efficiency by cake layers under optimal conditions was validated using both natural water sources and synthetic feed water. This work provides references for both research and engineering applications of direct microfiltration in high-turbidity water treatment.

2 Materials and methods

2.1 Experimental materials and solution configuration

Kaolin (6000 mesh, analytical grade) was purchased from Shanghai Yuanjiang Chemical Co., Ltd, $FeCl_3$ (analytically pure) was purchased from Shandong West Asia Chemical Industry Co., Ltd, humic acid (HA) was purchased from Shanghai McLean Biochemical Science and Technology Co., Ltd, and PVDF microfiltration membranes (pore size 0.22 μm, membrane diameter 50 mm) were purchased from Defilter Technology Co., Ltd. A certain amount of kaolin powder was dissolved in deionized water, transferred into a 3 L transparent plastic bucket, and shaken well. An appropriate amount of kaolin solution was taken to measure turbidity (repeated 5 times, with the average value taken), and kaolin solutions of different turbidities were prepared by dilution with water, and 1 g of HA was put into 1 L of deionized water, and then it was fully stirred and then fixed with a 1 L volumetric flask to obtain 1 g L^{-1} of HA solution.

2.2 Experimental setup and procedures

2.2.1 Experimental setup. The schematic diagram of the experimental setup is shown in Fig. 1, primarily consisting of

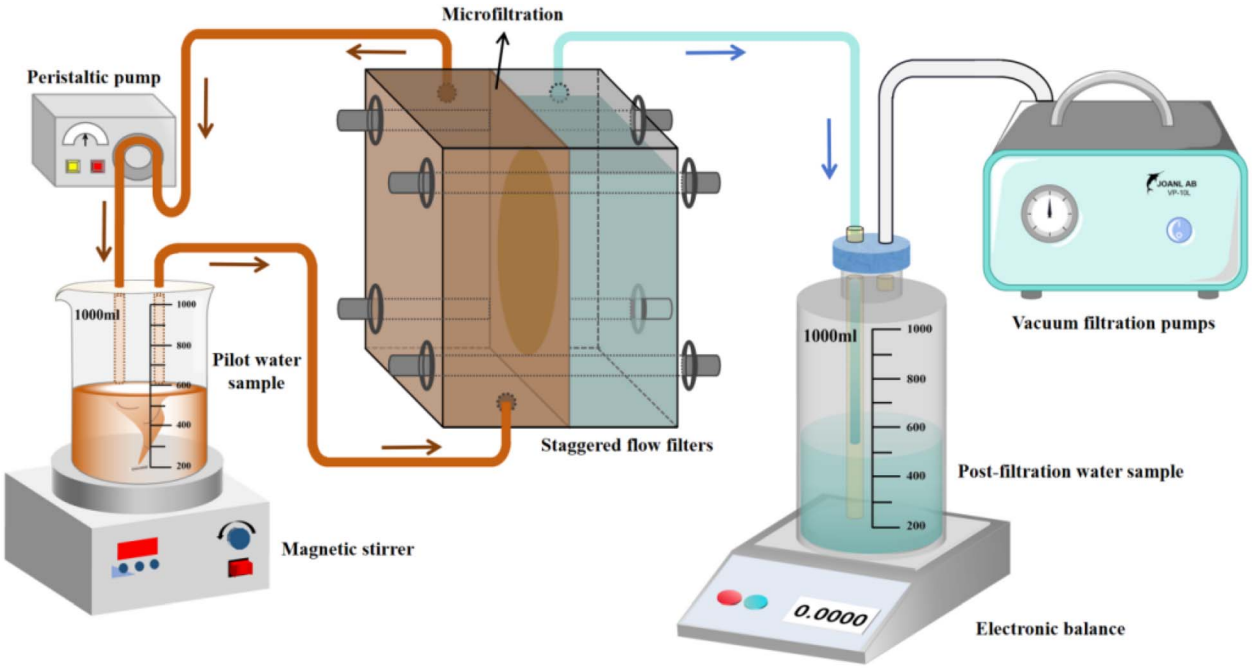

Fig. 1 Schematic diagram of the experimental setup.

a filtration device, vacuum filtration pump, peristaltic pump, filtration flask, beaker, magnetic stirrer, electronic balance, and silicone tubing.

2.2.2 Experimental procedures. Before starting the experiment, the filtration device, filtration flask, and silicone tubing should be rinsed with deionized water to avoid introducing impurities; after connecting all components, turn on the vacuum pump and check the airtightness of the setup. Monitor the pressure gauge to ensure pressure stability. If there is a difference between the pressure shown in the pressure gauge and the preset pressure for the test, the pressure can be controlled by turning the 4 screws of the filter unit. Set the sampling interval of the electronic balance to 15 seconds, perform filtration for 30 minutes, and use the four data points generated per minute as one cycle.

Each set of experiments requires testing the pure water flux (J_0), filtration flux (J_1), and backwash membrane flux (J_2). The specific experimental steps are as follows: (1) pure water flux test: filter 1 L of pure water, record the mass change of the filtered water using an electronic balance, and calculate the filtration flux. After the test, remove the membrane and inspect its surface for impurities. If no impurities are present, the pure water flux is accurate. (2) Filtration flux test: place the prepared high-turbidity water sample into a beaker (1 L), set the stirrer speed to 100 rpm, stir for 10 minutes, and begin filtration once the kaolin particles are evenly distributed in the water sample. Calculate the filtration flux based on data changes from the electronic balance. After cross-flow filtration, reverse the flow direction using the peristaltic pump to expel impurities deposited in the filtration device. Flip the filtration device to position the cake layer side upward, then turn off the vacuum pump and open the filtration device to remove the membrane with the cake layer. For dead-end filtration, the membrane can be directly removed after the experiment. (3) Backwash membrane flux test: remove the cake layer from the membrane surface, gently rinse it with deionized water, and reinstall the cleaned membrane into the filtration device. Subsequent steps are the same as in (1).

2.3 Analytical methods

2.3.1 Measurement of turbidity. The turbidity of the prepared high-turbidity water solution, test water samples, and filtered effluent was measured using a turbidimeter (WGZ-20, Shanghai, China). Due to the high turbidity of the samples, each measurement was repeated 3–5 times, and the average value was taken to ensure data stability. UV_{254} in water was measured using a UV spectrophotometer (UV2600A, Shanghai, China). The instrument required 30-minute preheating before measurement. Water samples were filtered through 0.45 μm membranes before testing. Measurements were conducted at 254 nm wavelength after filtration.

2.3.2 Measurement of filtration flux. Filtration flux is the volume of water passing through a unit membrane area per unit time, calculated as shown in eqn (1)–(3):[18,19]

$$J_{t(T)} = \frac{\Delta w}{1000 \times A \times \Delta t} \quad (1)$$

In the equation: $J_{t(T)}$ is the filtration flux at temperature T, m h^{-1}; Δw is the mass of the filtrate, kg; Δt is the operating time, h; A is the filtration area of the cake layer, m^2.

Since temperature affects water viscosity, thereby influencing filtration flux, temperature correction is applied to convert the filtration flux under various conditions to the flux at 25 °C. The conversion formula is as follows:

$$J_{25} = J_T \times \frac{\mu_r}{\mu_{25}} \quad (2)$$

In the equation: J_{25} is the filtration flux at 25 °C, m h^{-1}; J_T is the filtration flux at temperature T, m h^{-1}; μ_{25} is the dynamic viscosity coefficient of water at 25 °C, Pa s; μ_T is the dynamic viscosity coefficient of water at temperature T, Pa s. The dynamic viscosity coefficient of water at temperature T, μ_T, is calculated using eqn (3):[20]

$$\mu_T = \frac{1}{10} \times \frac{1}{2.1482 \times \left[T + 273.15 - 281.585 + \sqrt{8078.4 + (T + 273.15 - 281.585)^2}\right] - 120} \quad (3)$$

2.3.3 Analysis of membrane resistance composition. Research shows that the Darcy's law filtration model can fully demonstrate the relationship between membrane filtration flux, filtration pressure, and total resistance. In this experiment, the total membrane filtration resistance (R_t) is primarily composed of intrinsic membrane resistance (R_m), cake layer resistance (R_c), and membrane pore blockage resistance (R_f). Since the particle size of pollutants in water reaches the micron level after flocculation, the concentration polarization resistance (R_p) caused by thermal motion is not considered here. Among them, reversible membrane fouling (R_r) is composed of cake layer resistance, while irreversible membrane fouling (R_{ir}) is composed of membrane pore blockage resistance. The specific calculation formulas are shown in eqn (4) and (5).[21–23]

$$J = \frac{\Delta P}{\mu R} \quad (4)$$

$$R_t = R_m + R_c + R_f = R_r + R_{ir} \quad (5)$$

In the equation: J is the membrane filtration flux, m h^{-1}; ΔP is the filtration pressure, kPa, which in this experiment is the transmembrane pressure difference; μ is the viscosity coefficient, Pa s, taken as 1.005×10^{-3} in this experiment; R is the operating resistance, m^{-1}.

2.3.4 Measurement of cake layer porosity. After membrane filtration, use a spatula to collect the cake layer deposited on the membrane surface into a glass dish. Place the dish on an electronic balance to measure the wet weight of the cake layer (m_w). Then, transfer the weighed cake layer into an oven and dry it at 80 °C for 4 hours before weighing again to obtain the dry weight of the cake layer (m_d). Using the wet weight (m_w) and dry weight (m_d) of the cake layer, a material balance equation system is established. By solving this system, the dynamic membrane porosity calculation formulae can be derived as shown in eqn (6)–(8):[24,25]

$$V_w(1 - \varepsilon)\rho_s = m_d \quad (6)$$

$$V_w \varepsilon \rho_1 = m_w - m_d \quad (7)$$

$$\varepsilon = \frac{(m_w - m_d)\rho_s}{m_d\rho_1 + (m_w - m_d)\rho_s} \quad (8)$$

In the equation: V_w is the wet membrane volume (m^3); ε is the porosity of the cake layer; ρ_s is the density of suspended particles (g cm^{-3}), with kaolin density in this experiment being 2.6 g cm^{-3}; ρ_1 is the density of water, 1 g cm^{-3}.

2.3.5 Hermia model fitting. The Hermia model is generally suitable for studying membrane filtration processes under constant pressure and is used to determine the primary fouling mechanisms under different experimental conditions. The general equation expression of the Hermia model is as follows:[26]

$$\frac{d^2t}{dV^2} = k\left(\frac{dt}{dV^2}\right)^n \quad (9)$$

Depending on the value of n, the fouling mechanisms can be categorized into cake formation, intermediate blocking, standard blocking, and complete blocking. After linearizing the different equations, the analysis becomes more convenient, and the results are shown in Table 1.[27]

3 Results and discussion

3.1 Effect of turbidity on direct microfiltration treatment of high-turbidity feed water

Turbidity indicates the cloudiness or clarity of a liquid and is one of the primary indicators of water quality. It is sensitive to any suspended solids present and can directly reflect the amount of suspended particles in water.[28,29] To investigate the effect of turbidity on the direct treatment of high-turbidity water using microfiltration, this study prepared four high-turbidity water samples with turbidities of 300, 900, 1500, and 2100 NTU. Dead-end filtration was conducted for 30 minutes at a constant filtration pressure of 26.66 kPa, followed by backwashing and repeated filtration for a total of 5 cycles. The results of filtration flux and backwash membrane flux are shown in Fig. 2.

Table 1 Linear equations of the Hermia model (the fitting correlation results (R^2) are shown in Fig. 9)

Blocking mechanism	Linear equations
Complete blocking	$\ln(J^{-1}) = \ln(J_0^{-1}) + kt$
Standard blocking	$J^{-1/2} = J_0^{-1} + kt$
Intermediate blocking	$J^{-1} = J_0^{-1} + kt$
Cake layer blocking	$J^{-2} = J_0^{-2} + kt$

Analysis of membrane flux changes under different operating conditions reveals that the filtration flux variation can be divided into three stages: rapid decline, slow decline, and stable change, represented in this study by blue, green, and yellow, respectively. As shown in Fig. 2(a_1–d_1), the stability of repeated filtration (5 cycles) increases with higher influent turbidity. At an influent turbidity of 300 NTU, the variation in filtration flux across the 5 cycles is significant, with high dispersion. The dispersion coefficients (coefficient of variation = standard deviation/mean) for filtration flux in different stages are 0.1688, 0.2513, and 0.2402, respectively, which are much higher than those for the other three influent turbidities. As shown in Fig. 2(a_2–d_2), when the influent turbidity is 300 NTU, the average membrane flux recovery rate for repeated filtration is 80.18%, lower than those for 900 NTU (85.50%), 1500 NTU (83.49%), and 2100 NTU (86.47%). Additionally, the dispersion coefficient of the flux recovery rate is higher than those for the other three turbidities. The analysis reveals that at higher influent turbidity, inorganic particles in the water can quickly form a cake layer on the membrane surface, effectively blocking the impact of inorganic particles on the membrane and providing good protection. However, at lower influent turbidity, the cake layer formed on the membrane surface is thinner and looser, unable to effectively intercept subsequent inorganic particles, allowing them to pass through the cake layer and clog membrane pores, causing membrane fouling. It should be noted that while high-turbidity influent can quickly form a cake layer on the membrane surface, an excessively thick cake layer can cause a rapid decline in membrane flux, affecting filtration efficiency. Therefore, in the direct microfiltration of high-turbidity water, both membrane fouling and filtration flux must be considered.

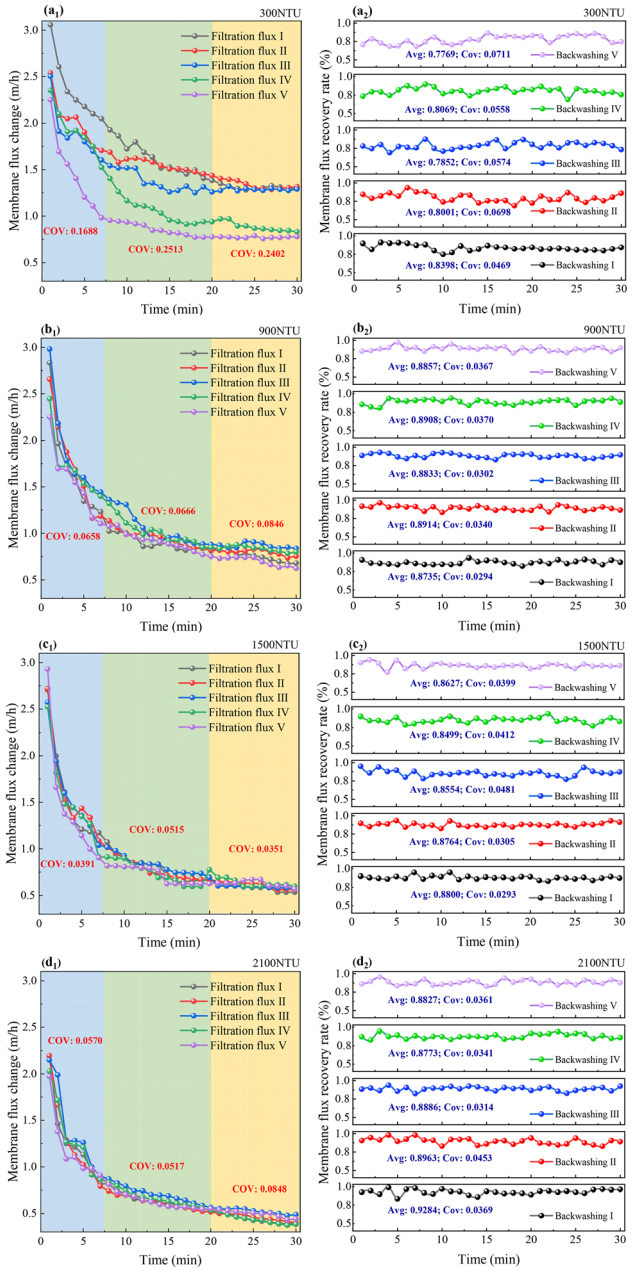

Fig. 2 Filtration flux and backwash membrane flux under different turbidities, (a) filtration flux changes (a_1)–(d_1); (b) backwash membrane flux (a_2)–(d_2).

3.2 Effect of filtration mode on direct microfiltration treatment of high-turbidity feed water

Cross-flow filtration refers to the process where, under pressure, the feed liquid flows at a certain velocity along the surface of the filtration medium, with particles in the feed liquid being retained on the surface of the medium, while the permeate passes through the medium. Unlike traditional dead-end filtration, cross-flow filtration involves the feed liquid flowing at an angle to the permeate flow direction, which reduces particle accumulation on the filtration medium surface, improving filtration efficiency and extending the lifespan of the filtration medium.[30,31] To investigate the impact of different filtration methods on the direct treatment of high-turbidity influent using microfiltration, this study employed both cross-flow and dead-end filtration at a transmembrane pressure of 26.66 kPa. High-turbidity water samples with turbidities of 100 NTU, 500 NTU, 900 NTU, and 1300 NTU were directly filtered for 30 minutes. The flux changes for the two filtration methods are shown in Fig. 3, and the membrane flux recovery rates are illustrated in Fig. 4.

Analysis of Fig. 3(a) reveals that under dead-end filtration, as the influent turbidity increases, the stable filtration flux gradually decreases, indicating that the thicker the cake layer structure on the membrane surface, the greater its negative impact on stable filtration flux. Analysis of Fig. 3(b) shows that as influent turbidity increases, the stable filtration flux exhibits a fluctuating pattern of first decreasing, then increasing, and then decreasing again. This indicates that with cross-flow filtration, the combined effect of gravity and water flow can reduce the thickness of the cake layer, preventing it from continuously increasing. Analysis of the reasons reveals that in dead-end filtration at lower influent turbidity, the cake layer formed on the membrane surface is thinner. Under the combined action of gravity and transmembrane pressure, the

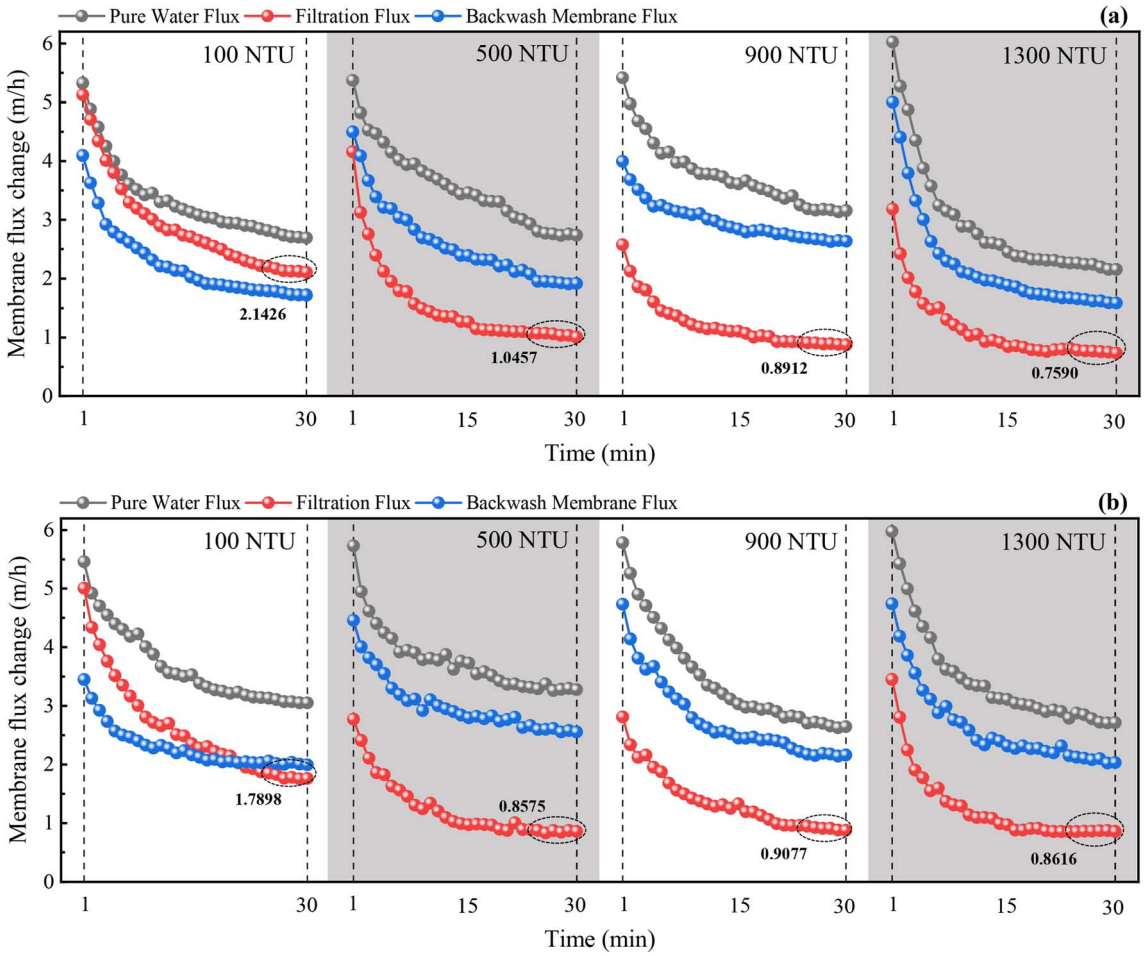

Fig. 3 Flux changes under different filtration methods, (a) dead-end filtration; (b) cross-flow filtration.

stable filtration flux is higher than that of cross-flow filtration, which relies solely on transmembrane pressure. At higher influent turbidity, the cake layer thickness in dead-end filtration is greater, significantly negatively impacting filtration flux. In cross-flow filtration, the cake layer thickness is reduced due to the combined effects of gravity and water flow on inorganic particles, resulting in a higher filtration flux compared to dead-end filtration.[32]

Analysis of Fig. 4 reveals that under different influent turbidities, the membrane flux recovery rate of dead-end filtration is only higher than that of cross-flow filtration at 100 NTU, and its dispersion coefficient is consistently higher than that of cross-flow filtration. This indicates that cross-flow filtration generates less membrane fouling when directly treating high-turbidity water, resulting in more stable filtration flux compared to dead-end filtration. At the same time, as the influent turbidity increases, the membrane flux recovery rate gradually rises, indicating that the cake layer structure formed by high-turbidity influent can effectively mitigate membrane fouling and ensure membrane flux recovery. However, it is important to consider the balance between membrane flux recovery rate and filtration efficiency, rather than pursuing only one of them. Therefore, considering both filtration flux and membrane flux recovery rate, cross-flow filtration should be adopted when directly treating high-turbidity water with microfiltration.

3.3 Effect of transmembrane pressure difference on direct microfiltration treatment of high-turbidity feed water

Transmembrane pressure difference refers to the pressure difference across the membrane during filtration. It is the driving force that pushes liquid through the membrane, directly affecting filtration speed and efficiency.[33] A larger transmembrane pressure difference can increase filtration speed but may also lead to membrane damage and fouling, while a smaller transmembrane pressure difference can result in excessively low filtration flux, affecting filtration efficiency.[34] To investigate the effect of different transmembrane pressure differences on the direct microfiltration treatment of high-turbidity water, this study set five transmembrane pressure differences: 6.67 kPa, 13.33 kPa, 20.00 kPa, 26.66 kPa, and 33.33 kPa. Using cross-flow filtration, high-turbidity water samples (900 NTU) were directly filtered for 30 minutes, with specific results shown in Fig. 5.

The microfiltration membrane used in this study has a pore size of 0.22 μm, and the average particle size of kaolin in the

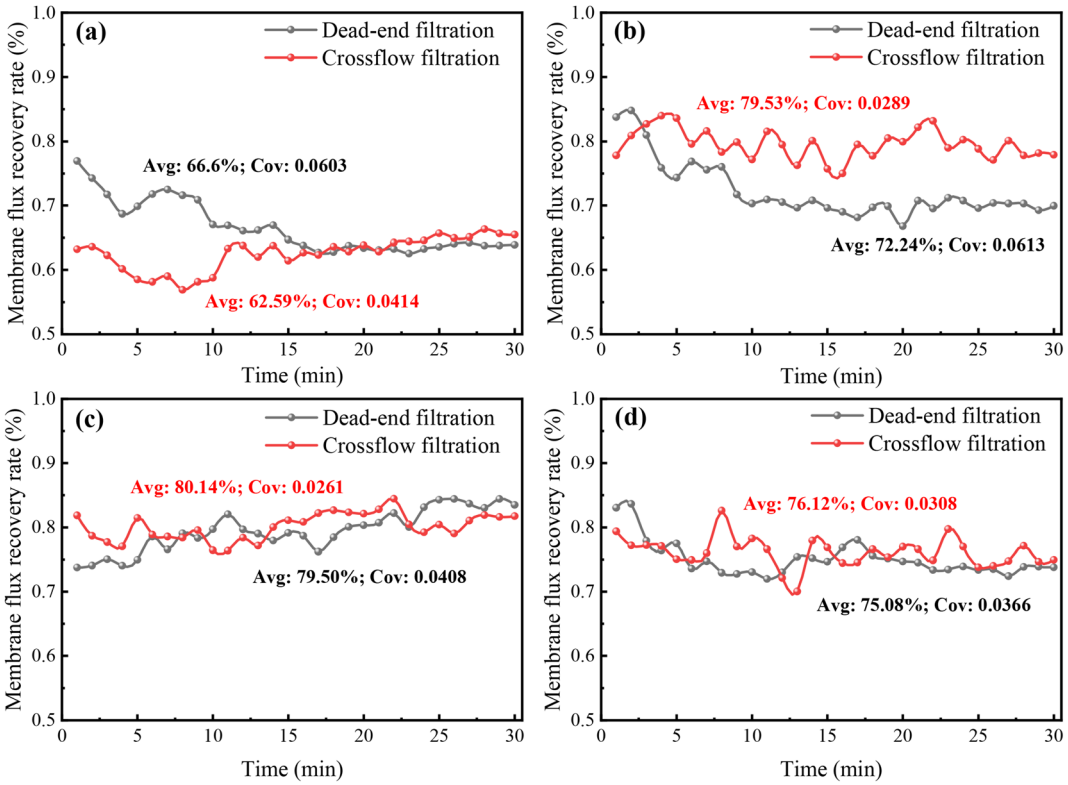

Fig. 4 Membrane flux recovery rates under different filtration methods, (a) 100 NTU; (b) 500 NTU; (c) 900 NTU; (d) 1300 NTU.

high-turbidity water samples is 11 μm. Therefore, when directly filtering high-turbidity water samples, the turbidity removal rate is typically maintained above 96% (Fig. 5(f)). As shown in Fig. 5, with the increase in transmembrane pressure difference, the stable filtration flux first decreases and then increases. At transmembrane pressure differences of 13.33 kPa and 33.33 kPa, the membrane flux recovery rates reach their maximum values of 87.11% and 65.88%, respectively. Analysis reveals that at a lower transmembrane pressure difference (6.67 kPa), kaolin particles in the influent are significantly influenced by water flow and gravity, preventing the rapid formation of a cake layer structure on the membrane surface that effectively blocks particle impact. This results in a lower membrane flux recovery rate (72.23%). As the transmembrane pressure difference increases (13.33 kPa), the thickening rate of the cake layer structure accelerates under pressure, forming an effective cake layer that protects the membrane. The cake layer structure also has a certain porosity, ensuring a relatively stable filtration flux. As the transmembrane pressure difference continues to rise (20.00 kPa), the increased pressure further compresses the cake layer structure, causing a slight decrease in stable filtration flux. Additionally, the higher transmembrane pressure difference intensifies the impact of particles on the membrane, exacerbating membrane fouling and reducing the membrane flux recovery rate (69.01%). When the transmembrane pressure difference is 26.66 kPa, the impact load of particles on the membrane surface increases further. However, the rapid formation of a cake layer of a certain thickness can effectively protect the membrane and reduce membrane fouling. When the transmembrane pressure difference increases to 33.33 kPa, the pressure effect far exceeds that of water flow and gravity, leading to rapid thickening of the cake layer. However, excessive pressure causes continuous compression of the cake layer, even partial fragmentation. While this ensures a higher stable filtration flux, membrane fouling is also higher, resulting in a lower membrane flux recovery rate (65.88%). From this, it can be concluded that transmembrane pressure difference has a dual effect on membrane fouling. On one hand, it increases the impact of inorganic particles in water on the membrane, exacerbating fouling. On the other hand, it facilitates the rapid formation of a cake layer of a certain thickness, blocking subsequent particle impacts and protecting the membrane. Moreover, when the pressure effect far exceeds gravity and water flow, cross-flow filtration loses its significance. Therefore, considering the impact load, cake layer structure, and stable filtration flux, this study selects 13.33 kPa as the optimal transmembrane pressure difference.

3.4 Analysis of membrane fouling resistance

3.4.1 Different turbidities. To further investigate the impact of turbidity on the direct treatment of high-turbidity water using microfiltration, this study analyzes the fouling resistance under different turbidities. The proportions and magnitudes of each fouling resistance are shown in Fig. 6, where Region I, II, and III represent membrane pore blockage

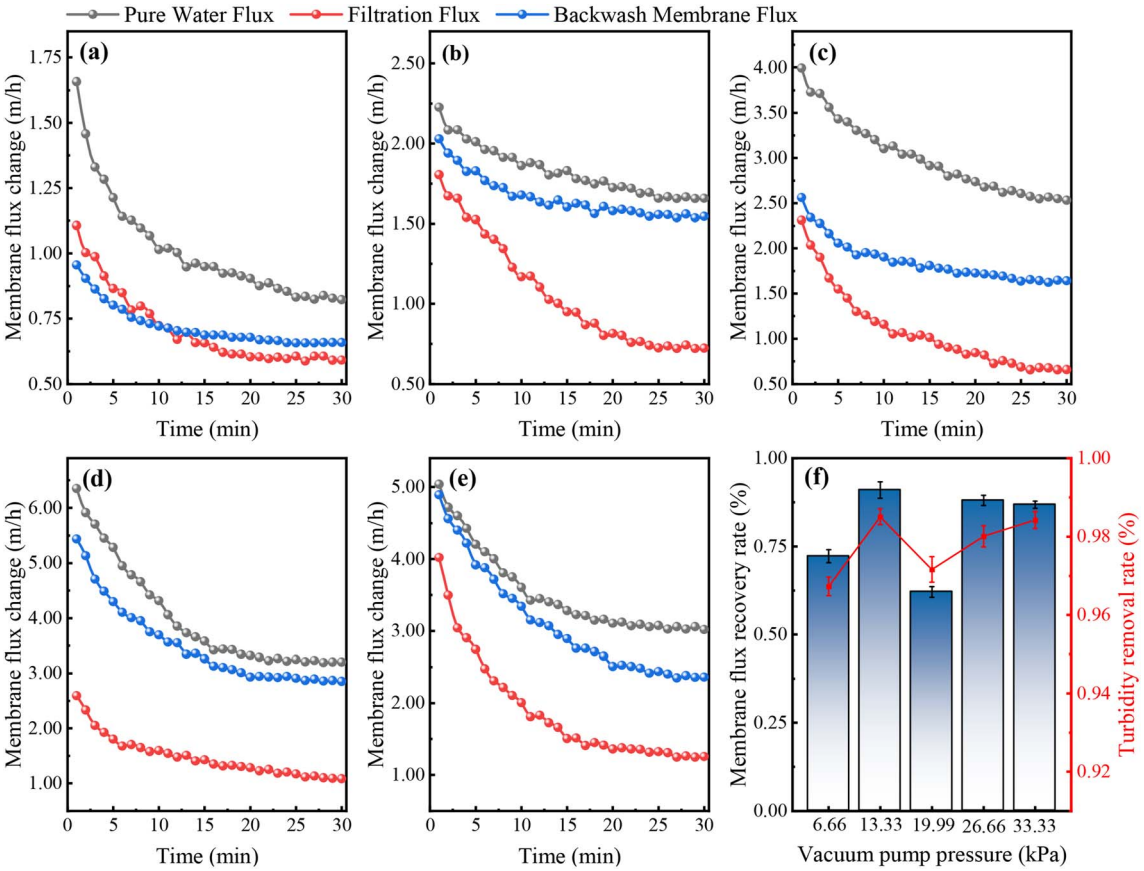

Fig. 5 Filtration flux changes under different transmembrane pressure differences, (a) 6.67 kPa; (b) 13.33 kPa; (c) 20.00 kPa; (d) 26.66 kPa; (e) 33.33 kPa; (f) membrane flux recovery rate and turbidity removal rate.

resistance, cake layer resistance, and intrinsic membrane resistance, respectively.

Analysis of Fig. 6 reveals that as influent turbidity increases, the proportion and magnitude of membrane pore blockage resistance generally decrease. At an influent turbidity of 100 NTU, the membrane pore resistance is 1.31×10^{10} m^{-1}, which is 27.18% higher than at 1500 NTU. The intrinsic membrane resistance remains relatively constant, while the total filtration resistance increases by 5.6×10^{10} m^{-1} with rising turbidity. The cake layer resistance increases by 5.86×10^{10} m^{-1}, indicating that the total filtration resistance is primarily driven by changes in cake layer resistance. The increase in turbidity does not exacerbate irreversible membrane fouling (Fig. 6(b)). The analysis reveals that at lower influent turbidity, particles in the water have a greater impact on the membrane, and the cake layer structure on the membrane surface forms more slowly, failing to provide timely protection. As a result, membrane fouling is higher, and the membrane flux recovery rate is lower. As the influent turbidity increases, the rate of cake layer thickening accelerates, and the cake layer effectively reduces the impact of particles on the membrane, leading to a gradual decrease in membrane fouling. Therefore, although an increase in influent turbidity reduces filtration flux, it effectively decreases irreversible membrane fouling and extends membrane lifespan. The discrepancy with other researchers' conclusions may be due to the fact that the high-turbidity water samples in this study contain only kaolin particles, with an average particle size larger than the microfiltration membrane pore size.[35] When the influent turbidity increases from 100 NTU to 1500 NTU, the membrane pore blockage resistance decreases by 21.37%, while the total filtration resistance doubles. At an influent turbidity of 900 NTU, the membrane pore blockage resistance decreases by 22.14%, and the total filtration resistance increases by only 37.1%, indicating that the treatment of high-turbidity water samples at 900 NTU yields the best results in this study. Therefore, when directly treating high-turbidity water with microfiltration, the optimal high-turbidity water samples that different scales of experimental setups can handle vary, and it is necessary to select the most cost-effective treatment target.

3.4.2 Different filtration methods. To further investigate the impact of filtration methods on the direct treatment of high-turbidity water using microfiltration, this study analyzes the fouling resistance under dead-end filtration and cross-flow filtration. The proportions and magnitudes of each fouling resistance are shown in Fig. 7, where Region I, II, and III represent membrane pore blockage resistance, cake layer resistance, and intrinsic membrane resistance, respectively.

Analysis of Fig. 7 reveals that as influent turbidity increases, the magnitude and proportion of membrane pore blockage resistance under both filtration methods show a decreasing trend. Compared to an influent turbidity of 100 NTU, at 1300 NTU, the reduction in membrane pore blockage resistance for

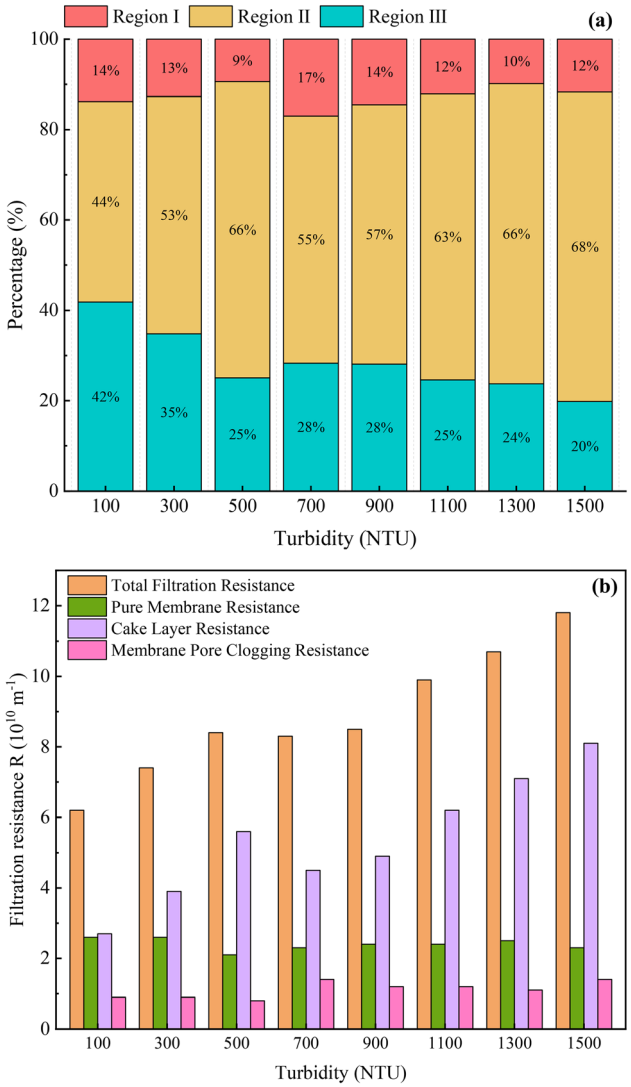

Fig. 6 Changes under different turbidities, (a) proportion of membrane fouling types; (b) variations in membrane fouling resistance.

dead-end filtration is 13.9%, lower than that for cross-flow filtration (24.79%). The increase in cake layer resistance is 67.68%, higher than that for cross-flow filtration (66.38%). At an influent turbidity of 900 NTU, the membrane pore blockage resistance for dead-end filtration is 1.07×10^{10} m^{-1}, 10.31% higher than that for cross-flow filtration. Analysis shows that the changes in total resistance for both filtration methods are primarily caused by the increase in cake layer resistance, consistent with the conclusions drawn from Fig. 6. When using cross-flow filtration to treat high-turbidity water, particles in the water are influenced by gravity and water flow, preventing them from entirely depositing on the membrane to form a cake layer. This reduces the impact of particles on the membrane and mitigates membrane fouling. Therefore, cross-flow filtration results in lower membrane pore blockage resistance compared to dead-end filtration when treating influent of varying turbidities. Additionally, under the influence of gravity and water flow shear forces, cross-flow filtration can effectively control the thickness of the cake layer, reducing the total filtration resistance. Therefore, in high-turbidity water treatment, considering both membrane fouling resistance and stable filtration flux, cross-flow filtration is recommended as the most suitable method.

3.4.3 Different transmembrane pressure differences. To further investigate the impact of transmembrane pressure differences on the direct treatment of high-turbidity water using microfiltration, this study analyzes the fouling resistance at 6.66 kPa, 13.33 kPa, 20.00 kPa, 26.66 kPa, and 33.33 kPa. The proportions and magnitudes of each fouling resistance are shown in Fig. 8, where Region I, II, and III represent membrane pore blockage resistance, cake layer resistance, and intrinsic membrane resistance, respectively.

Analysis of Fig. 8(a) shows that as the transmembrane pressure difference increases, the proportion of membrane pore blockage resistance generally decreases but exhibits fluctuations. At a transmembrane pressure difference of 6.66 kPa, the membrane pore resistance is 24%, which is 9% lower than at 33.33 kPa. At 26.66 kPa, the proportion of membrane pore blockage resistance is the lowest at 12%. This indicates that as pressure increases, the contribution of membrane pore blockage to total resistance gradually decreases. The proportion of cake layer resistance significantly increases with higher transmembrane pressure differences. When the pressure rises from 6.66 kPa to 33.33 kPa, the proportion of cake layer resistance increases by 33%, indicating that at higher pressures, the formation and thickening of the cake layer contribute more significantly to the total filtration resistance. Analysis of Fig. 8(b) reveals that the total filtration resistance significantly increases with higher transmembrane pressure differences. At 33.33 kPa, the total filtration resistance reaches its maximum (9.89×10^{10} m^{-1}), representing a 100.61% increase compared to 6.66 kPa (4.93×10^{10} m^{-1}). The cake layer resistance follows the same trend as the total filtration resistance. When the pressure increases from 6.66 kPa to 33.33 kPa, the cake layer resistance rises by 4.62×10^{10} m^{-1}, an increase of 366.37%, further indicating that cake layer resistance is the primary cause of changes in total resistance. The membrane pore blockage resistance generally shows an increasing trend with higher transmembrane pressure differences. At a pressure of 13.33 kPa, the membrane pore blockage resistance is the lowest, at only 0.94×10^{10} m^{-1}. The analysis reveals that at lower pressures, an effective cake layer structure cannot form to protect the membrane. At excessively high pressures, not only does the impact of particles on the membrane increase, but the cake layer structure may also collapse and break, exacerbating membrane fouling.[36] At a transmembrane pressure difference of 13.33 kPa, the effects of gravity and water flow shear on the cake layer thickness are significant. This not only ensures a certain cake layer thickness to protect the membrane but also prevents the cake layer from becoming too thick, which could affect filtration efficiency. Therefore, 13.33 kPa is considered the optimal transmembrane pressure difference in this study. It should be noted that changes in transmembrane pressure difference significantly affect the cake layer thickness in cross-flow filtration. Higher transmembrane pressure differences

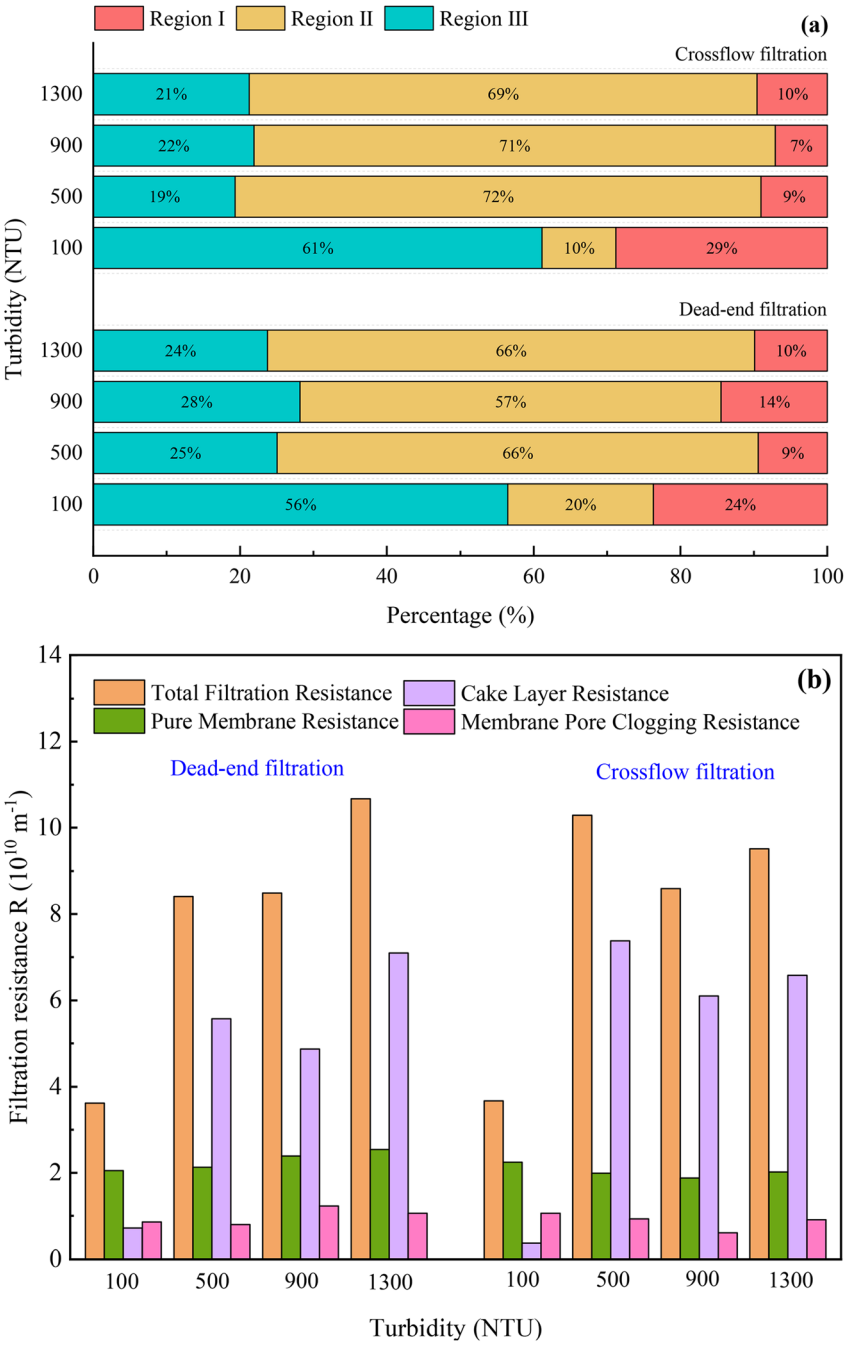

Fig. 7 Changes under different filtration methods, (a) proportion of membrane fouling types; (b) variations in membrane fouling resistance.

can impact the effectiveness of cross-flow filtration. In high-turbidity water treatment, it is not advisable to solely pursue high pressure for increased membrane flux; attention must also be paid to irreversible fouling issues, seeking a more balanced transmembrane pressure.

3.5 Fitting with the Hermia classical model

The Hermia model is one of the commonly used models for analyzing membrane fouling mechanisms. It categorizes membrane fouling into four blocking mechanisms: complete blocking, standard blocking, intermediate blocking, and cake layer blocking, and can accurately identify the primary causes of membrane fouling during filtration.[37,38] To investigate the effects of turbidity, filtration method, and transmembrane pressure difference on the direct treatment of high-turbidity water using microfiltration, this study employs the Hermia model to perform linear correlation (R^2) fitting for the filtration system under different operating conditions. The results are shown in Fig. 9.

Analysis of the filtration methods in Fig. 9 reveals that with dead-end filtration, as influent turbidity increases, membrane fouling exhibits three types: complete blocking (100 NTU, 500

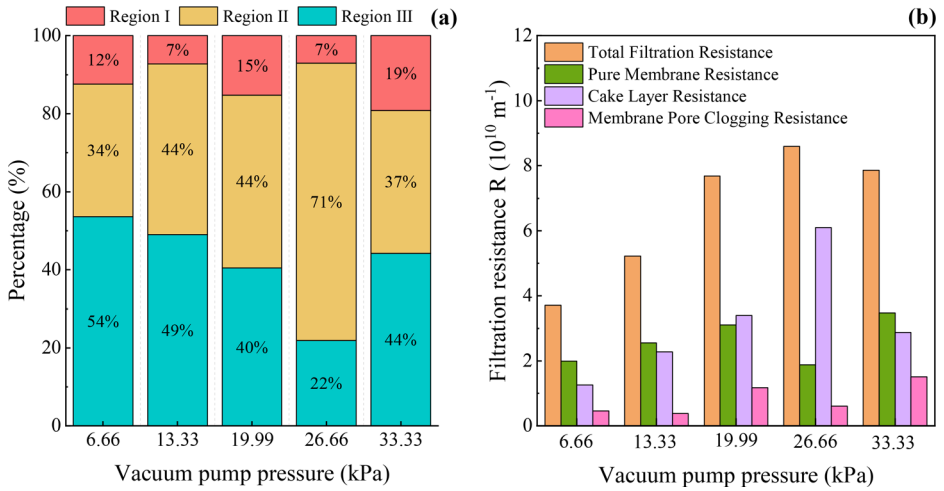

Fig. 8 Changes under different transmembrane pressure differences, (a) proportion of membrane fouling types; (b) variations in membrane fouling resistance.

NTU), standard blocking (1300 NTU), and cake layer blocking (900 NTU). With cross-flow filtration, four types of membrane fouling occur: complete blocking (100 NTU), standard blocking (500 NTU), intermediate blocking (1300 NTU), and cake layer blocking (900 NTU). Both filtration methods show cake layer blocking at 900 NTU. The analysis shows that during dead-end filtration, at lower influent turbidity (100 NTU and 500 NTU), particles in the water exert a greater impact on the membrane due to pressure and gravity. Smaller particles in the water enter and completely block the membrane pores, intensifying membrane fouling and causing complete blocking fouling. As the influent turbidity increases (900 NTU), the cake layer structure thickens rapidly to reduce the impact of particles on the membrane. Although the membrane thickens slowly, the cake layer has a certain spatial structure internally. Although smaller particles in the influent continue to fill the cake layer structure, their limited quantity does not cause significant membrane fouling. Instead, they enhance the filtration efficiency and compressive strength of the cake layer, resulting in cake layer blocking. With further increases in influent turbidity (1300 NTU), the concentration of particles in the influent rises significantly, causing the cake layer to continuously compact

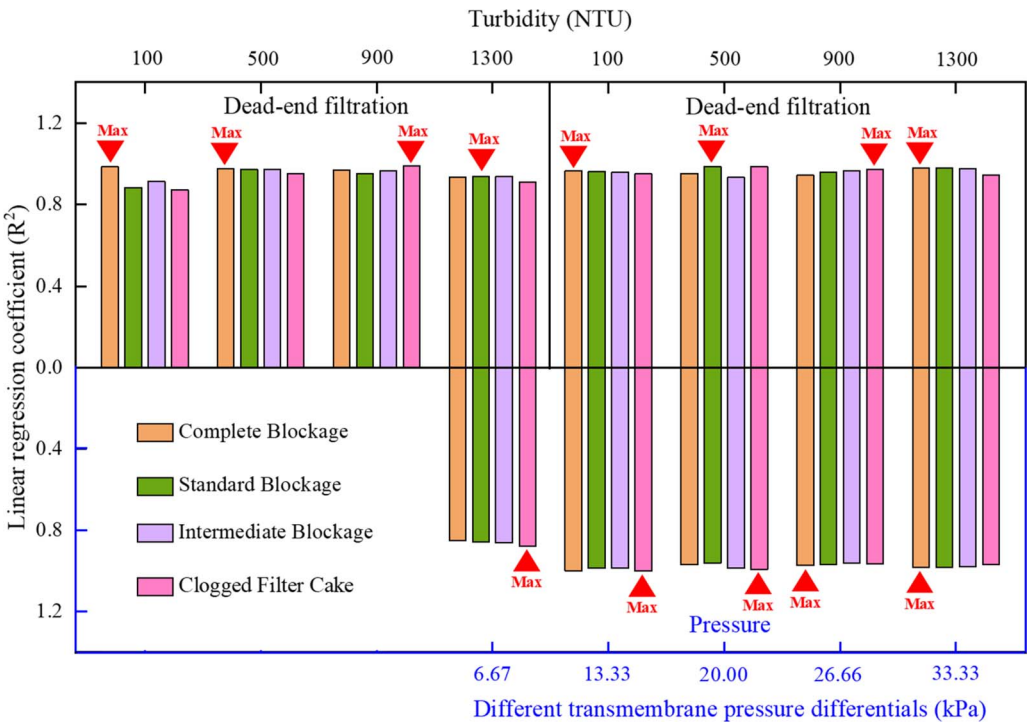

Fig. 9 Hermia model fitting under different filtrationmethods and transmembrane pressure differences.

and thicken. Smaller particles, under higher pressure, impact the membrane, leading to intermediate blocking filtration.[39] Analysis of the transmembrane pressure differences in Fig. 9 reveals that as pressure increases, membrane fouling exhibits two types of blocking: cake layer blocking and complete blocking. Only at 33.33 kPa does complete blocking occur, while cake layer blocking is observed at other pressures. The analysis shows that at 33.33 kPa, the extremely high pressure continuously compresses the cake layer structure, even causing it to collapse. This allows smaller particles in the water to impact the membrane, leading to severe membrane fouling. It should be noted that at lower pressures, although the impact of influent particles is reduced, the cake layer structure forms thinly and loosely. Therefore, it is necessary to consider both the blocking type and irreversible membrane fouling to select an appropriate transmembrane pressure.

3.6 Porosity analysis

The porosity of the cake layer affects filtration primarily in terms of filtration speed, filtration resistance, filtrate quality, and cake compressibility. When treating the same water sample, lower cake layer porosity results in higher filtration resistance, lower filtration flux, and reduced cake compressibility.[40] To further investigate the effects of turbidity, filtration method, and transmembrane pressure difference on the direct treatment of high-turbidity water using microfiltration, this study calculates the porosity of the cake layer under different operating conditions. The specific results are shown in Fig. 10.

As shown in Fig. 10(a), as the influent turbidity increases, the porosity of the cake layer shows a gradual declining trend. When the influent turbidity rises from 100 NTU to 1500 NTU, the porosity decreases by 3.79%, but the rate of decline gradually changes and approaches zero. As the transmembrane pressure difference increases, the porosity decreases almost linearly. When the transmembrane pressure difference rises from 6.67 to 33.33, the porosity decreases by 13.53%. The analysis reveals that under constant transmembrane pressure, when the particle content in the influent is low, the cake layer structure on the membrane surface is looser, with higher porosity and higher filtration flux. However, the cake layer formed at this time is thinner and cannot effectively protect the membrane, leading to higher membrane fouling. As the concentration of particles in the influent increases, the rate at which the cake layer thickens on the membrane surface accelerates. Under pressure, some smaller particles penetrate deeper into the cake structure, reducing the porosity of the lower layers and affecting filtration flux. However, the porosity of the upper layers of the cake structure increases, leading to a slower decline in overall porosity but a continuous decrease in filtration flux. It should be noted that higher influent turbidity indicates a greater number of smaller particles in the water, which more easily reduces the porosity of the deeper layers of the cake structure, affecting filtration flux. However, at lower turbidity, the cake structure is looser and thinner, causing porosity to decline rapidly. When constant pressure changes, as pressure increases, smaller particles penetrate deeper into the cake structure, and weaker particles are continuously compressed and broken, causing porosity to decrease until the cake structure develops high compressive strength. However, due to the large transmembrane pressure difference, filtration flux can still be maintained at a high level.

Analysis of Fig. 10(b) reveals that as influent turbidity increases, the porosity under both filtration methods shows a gradual decreasing trend. When cross-flow filtration is used, the cake layer porosity at different influent turbidities is higher than that of dead-end filtration. The analysis shows that during cross-flow filtration under constant pressure, particles in the water, influenced by gravity and water flow, can effectively

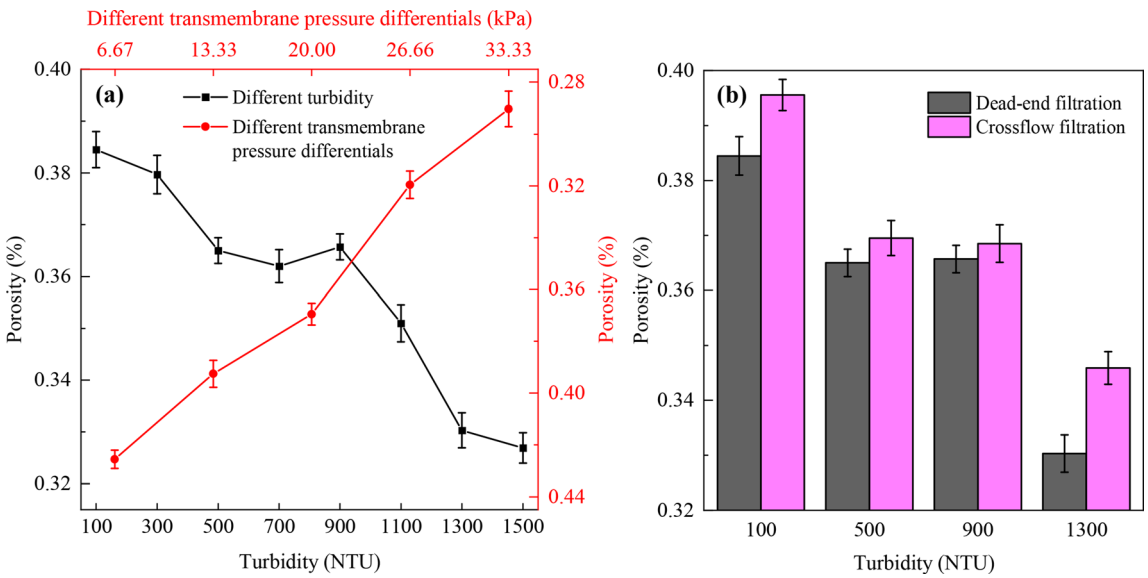

Fig. 10 Porosity under different conditions, (a) different influent turbidity and transmembrane pressure differences; (b) different filtration methods.

control the thickness of the cake layer, resulting in a cake layer structure with higher porosity. At the same time, as influent turbidity increases, cross-flow filtration also experiences smaller particles entering the cake layer. However, under the influence of gravity, larger particles are less likely to deposit on the membrane surface, resulting in a lower average particle size of deposited particles compared to dead-end filtration. Although the porosity of the cake layer structure is lower than that of dead-end filtration, it effectively prevents the entry of smaller particles, leading to higher porosity than dead-end filtration.

3.7 Cake layer regulation and performance validation

Investigations of varying turbidity levels, filtration modes, and transmembrane pressures revealed that the cake layer structure effectively intercepted influent contaminants, maintained higher flux, and mitigated membrane fouling. Consequently, $FeCl_3$ was employed as coagulant to regulate cake layer structure, with five dosage gradients (0, 5, 10, 15, 20 mg L^{-1}) under cross-flow filtration at 13.33 kPa transmembrane pressure. Variations in membrane flux, flux recovery rate, and turbidity removal efficiency at different $FeCl_3$ dosages are presented in Fig. 11.

As shown in Fig. 11, the pure water flux, filtration flux, and backwash flux all exhibited significant decreasing trends during filtration. With increasing $FeCl_3$ concentration, stable filtration flux gradually decreased from 0.7342 m h^{-1} at 0 mg L^{-1}, peaked at 0.6852 m h^{-1} with 15 mg per L $FeCl_3$, then declined again. This phenomenon occurs because insufficient coagulant at low $FeCl_3$ concentrations allows fine particles to directly contact the membrane, forming loose cake layers with initially high but rapidly declining flux. Increased $FeCl_3$ promotes coagulation between Fe^{3+} and dissolved organics/suspended solids, forming larger flocs that create denser yet more stable cake layers, reducing pore blockage while compromising hydraulic permeability. At 15 mg per L $FeCl_3$, floc characteristics achieve an optimal balance, creating cake layers that combine effective particle retention with maintained flux, resulting in peak performance. Excessive $FeCl_3$ causes oversized, heterogeneous flocs that form irregular cake layers with localized flow resistance, decreasing flux. Furthermore, excess Fe^{3+} may destabilize flocs, releasing fine particles and dissolved matter that exacerbate membrane fouling. Simultaneously, analysis revealed that the hydrophobicity and negative surface charge of PVDF membranes promoted humic acid adsorption and particle deposition, exacerbating irreversible fouling. In contrast, $FeCl_3$ coagulation optimized cake layer structure through charge neutralization and floc bridging, intercepting contaminants and reducing pore blockage. At 15 mg per L $FeCl_3$ dosage, the maximum flux recovery rate reached 88.77%. Thus, the optimal $FeCl_3$ dosage was determined to be 15 mg L^{-1}.

To further validate the effect of 15 mg per L $FeCl_3$ on cake layer formation. Experiments were performed using both natural water and synthetic feed water at this concentration. The experimental duration was extended by 50% to 45 minutes. The HA content in filtrate was determined for verification. The results are presented in Fig. 12 and Table 2.

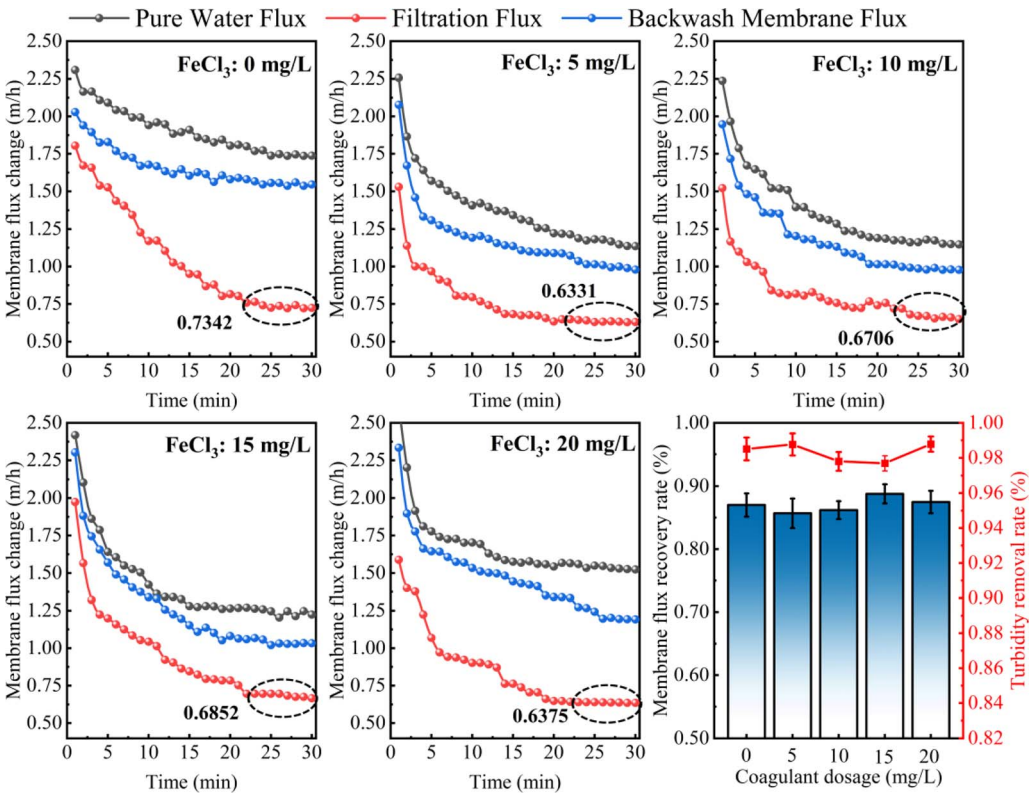

Fig. 11 Variations in membrane flux, flux recovery rate and turbidity removal efficiency at different $FeCl_3$ concentrations.

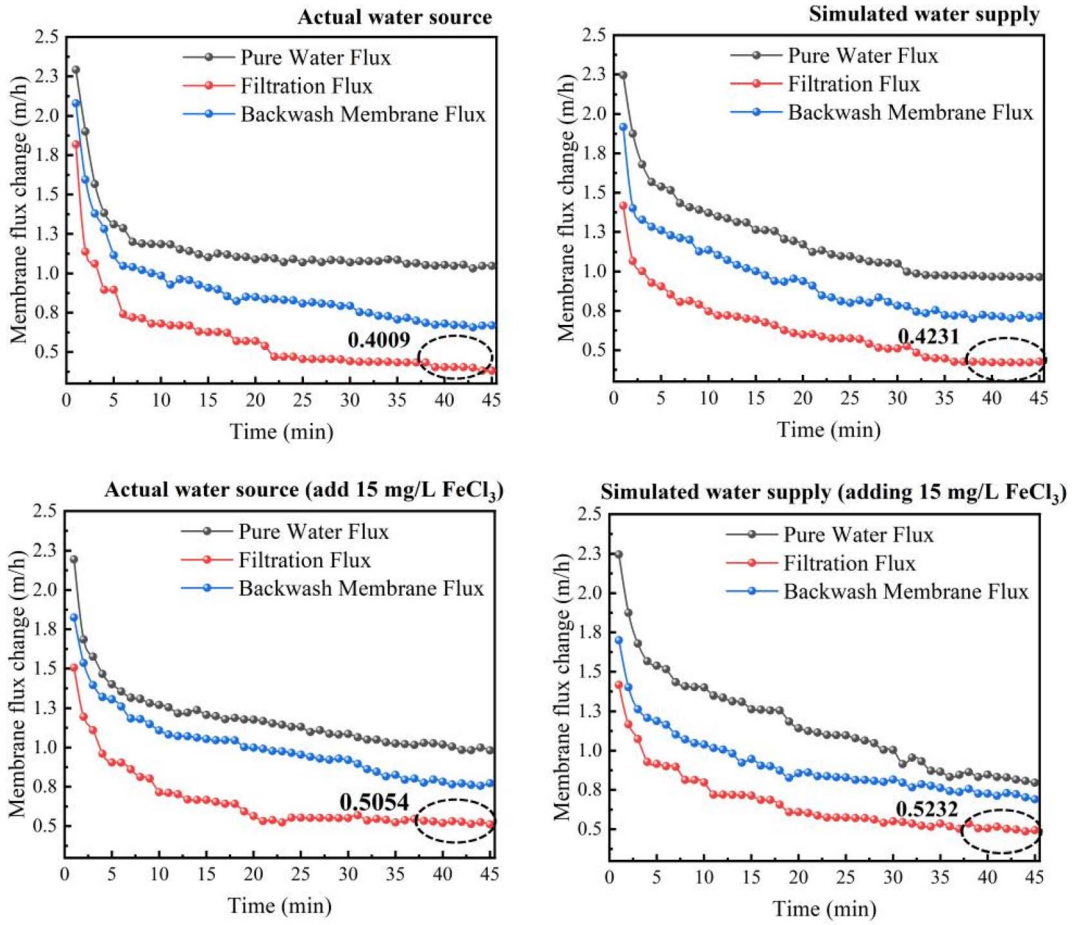

Fig. 12 Membrane flux changes of actual water source and simulated water under optimal conditions.

As shown in Fig. 12 and Table 2, the stable filtration flux of raw water without 15 mg per L $FeCl_3$ coagulant was 0.4009 m h^{-1}, with a post-filtration HA concentration of 2.09 mg L^{-1}, HA removal rate of 58.18%, and flux recovery rate of 75.49%. With 15 mg per L $FeCl_3$ coagulant, the stable filtration flux of raw water increased to 0.5054 m h^{-1}, post-filtration HA concentration decreased to 1.207 mg L^{-1}, HA removal rate reached 75.86%, flux recovery rate was 79.06%, and stable flux enhancement rate was 26.07%. For synthetic water without 15 mg per L $FeCl_3$ coagulant, the stable filtration flux was 0.4231 m h^{-1}, post-filtration HA concentration was 1.878 mg L^{-1}, HA removal rate was 62.44%, and flux recovery rate was 77.38%. With 15 mg per L $FeCl_3$ coagulant in synthetic water, stable filtration flux reached 0.5232 m h^{-1}, post-filtration HA concentration was 1.125 mg L^{-1}, HA removal rate was 77.44%, flux recovery rate was 84.31%, and stable flux enhancement rate was 23.66%. The analysis indicates that 15 mg per L $FeCl_3$ dosage forms a filter cake layer with high compressive strength and porosity, effectively removing pollutants and mitigating membrane fouling. Actual water sources contain diverse contaminants that progressively deposit on membrane surfaces and inside pores during filtration, creating a fouling layer. Simulated water is artificially formulated. Despite compositional similarities to actual water sources, its simpler nature increases coagulant responsiveness, promotes larger floc formation, and consequently improves filtration flux. Moreover, actual water sources contain not only HA but also other organic compounds and microorganisms that could compromise

Table 2 Humic acid removal efficiency and flux recovery rates across various water sources

	Effluent humic acid concentration (mg L^{-1})	HA removal efficiency	Flux recovery rate
Actual water source	2.09	58.18%	75.49%
Simulated water	1.878	62.44%	77.38%
Actual water source (15 mg per L $FeCl_3$ dosed)	1.207	75.86%	79.06%
Simulated water (15 mg per L $FeCl_3$ dosed)	1.125	77.44%	84.31%

coagulant-HA interaction efficiency. In simulated water, HA's limited structural diversity allows Fe^{3+} (from $FeCl_3$) to generate more stable flocs with homogeneous pore distribution and enhanced adsorption capability, achieving superior HA interception.

Investigations of actual and simulated water sources showed that a filter cake layer formed under 13.33 kPa transmembrane pressure, 15 mg per L $FeCl_3$ dosage, and cross-flow filtration achieved maximum contaminant removal efficiency, offering valuable insights for developing eco-friendly high-turbidity water treatment methods.

4 Conclusions

The research applied microfiltration technology for direct treatment of high-turbidity raw water. Through examining impacts of varying turbidity levels, filtration methods, transmembrane pressure differences, and $FeCl_3$ coagulant dosages on filtration efficiency, the study elucidated membrane fouling alleviation mechanisms to establish an environmentally sustainable water treatment approach. Key findings are summarized below.

(1) When using microfiltration to directly treat high-turbidity feed water, at lower influent turbidity (100 NTU), the cake layer structure is looser and cannot effectively protect the membrane. The irreversible membrane fouling is relatively high at 1.31×10^{10} m^{-1}, and the membrane flux recovery rate is lower. At higher influent turbidity (1300 NTU), irreversible fouling is only 1.04×10^{10} m^{-1}, but excessive particles in the water cause the cake layer structure to become too thick, with lower porosity, resulting in a filtration flux of only 35.42% of that at 100 NTU. Therefore, in high-turbidity water treatment, the optimal influent turbidity should be explored based on the specifications of the filtration equipment.

(2) Under constant pressure conditions, cross-flow filtration performs better than dead-end filtration when directly treating high-turbidity feed water. At influent turbidities of 500 NTU, 900 NTU, and 1300 NTU, the membrane flux recovery rate and irreversible membrane fouling of dead-end filtration are lower than those of cross-flow filtration. At an influent turbidity of 1300 NTU, the stable filtration flux of cross-flow filtration is 13.52% higher than that of dead-end filtration, and irreversible membrane fouling is only 81.98% of that of dead-end filtration. Therefore, this study concludes that cross-flow filtration is the superior choice for high-turbidity water treatment.

(3) At a constant influent turbidity (900 NTU), when the pressure increases from 6.66 kPa to 33.33 kPa, irreversible membrane fouling increases by 27.97%, and the cake layer porosity decreases by 13.53%, but the stable filtration flux increases by 116.91%. At a transmembrane pressure difference of 13.33 kPa, although the filtration flux is 56.83% of that at 33.33 kPa, irreversible membrane fouling is only 62.25%, and the membrane flux recovery rate is as high as 87.11%. Therefore, in high-turbidity water treatment, transmembrane pressure difference is the main factor causing membrane fouling and improving membrane flux, and 13.33 kPa is the optimal transmembrane pressure difference in this study.

(4) Analysis using the Hermia model reveals that at transmembrane pressure differences of 6.66 kPa, 13.33 kPa, 20.00 kPa, and 26.66 kPa, the blocking type is cake layer blocking. When the transmembrane pressure difference increases to 33.33 kPa, the blocking type shifts to complete blocking. This indicates that excessively high transmembrane pressure differences increase the impact of particles in the water on the membrane, exacerbating membrane fouling. Therefore, it is necessary to balance the relationship between membrane fouling and filtration flux, seeking more low-carbon and environmentally friendly process conditions.

(5) The research confirms $FeCl_3$ coagulant's ability to alleviate membrane fouling and improve flux stability through controlled filter cake layer formation. With 15 mg per L $FeCl_3$ addition, the engineered filter cake layer exhibited balanced rejection-permeability characteristics, delivering 0.6852 m h^{-1} stable flux and 88.77% recovery rate. Fe^{3+} at this dosage creates compact flocs *via* charge neutralization/bridging mechanisms, concurrently mitigating pore clogging by colloids and minimizing flow resistance. In actual water treatment, coagulant-enhanced systems achieved 17.68% higher HA removal than non-coagulant controls, with synthetic water demonstrating 15% enhancement. These results establish a theoretical framework for precise filter cake layer control in turbid water purification.

Data availability

All relevant data used in this study can be obtained from the corresponding authors upon reasonable request.

Author contributions

The conceptualization and methodological framework of this research were collaboratively developed by all contributing authors. Data acquisition, preparation of research materials, and analytical procedures were conducted under the supervision of Ping Li. The initial manuscript was drafted by Xiaosan Song, Qingchao Shen, Wenxuan Wei, and Hairong Yan, who subsequently incorporated revisions based on critical feedback provided by all co-authors. The final version of the manuscript represents a collective effort, having undergone rigorous review and approval by all participating authors prior to submission.

Conflicts of interest

No conflict of interest was reported by the authors.

Acknowledgements

This study was supported by the Research Program for Gansu Provincial Science and Technology Program (20JR10RA228).

References

1 P. Y. Li and H. Qian, Water resources research to support a sustainable China, *Int. J. Water Resour. Dev.*, 2018, **34**, 327–336.
2 J. H. Li, X. H. Lei, Y. Qian, *et al.*, The Water Status in China and an Adaptive Governance Frame for Water Management, *Int. J. Environ. Res. Public Health*, 2020, **17**, 2085.
3 X. Wang, Z. Wang, W. T. Yang, *et al.*, Current Status and Future Development Directions of Water Resources in China (China), *J. Environ. Eng.*, 2014, **32**, 1–5.
4 C. L. Chang and C. S. Liao, Assessing the risk posed by high-turbidity water to water supplies, *Environ. Monit. Assess.*, 2012, **184**, 3127–3132.
5 H. Tahraoui, S. Toumi, M. Boudoukhani, N. Touzout, A. Sid, A. Amrane, A. Belhadj, M. Hadjadj, Y. Laichi, M. Aboumustapha, M. Kebir, A. Bouguettoucha, D. Chebli and A. Assadi, Zhang. Evaluating the Effectiveness of Coagulation–Flocculation Treatment Using Aluminum Sulfate on a Polluted Surface Water Source: A Year-Long Study, *J. Water*, 2024, **16**, 400.
6 T. Ritigala, H. Demissie, Y. Chen, *et al.*, Optimized pretreatment of high strength food waste digestate by high content aluminum-nanocluster based magnetic coagulation, *J. Environ. Sci.*, 2021, **104**, 430–443.
7 M. Xu, W. B. Zhou, Z. Q. Zhu, *et al.*, Study on the preparation of polysilicate ferric flocculant and its treatment of high turbidity tailings water, *J. Water Process Eng.*, 2021, **44**, 102457.
8 T. M. Hessam, A sustainable approach for industrial wastewater treatment using pomegranate seeds in flocculation-coagulation process: Optimization of COD and turbidity removal by response surface methodology (RSM), *J. Water Process Eng.*, 2023, **53**, 103651.
9 M. Yan, D. Wang, J. Qu, J. Ni and C. Chow, Enhanced coagulation for high alkalinity and micro-polluted water: the third way through coagulant optimization, *Water Res.*, 2008, **42**, 2278–2286.
10 J. R. Werber, C. O. Osuji and M. Elimelech, Materials for next-generation desalination and water purification membranes, *Nat. Rev. Mater.*, 2016, **1**, 16018.
11 C. S. Ye, X. N. Song, Q. Qian, *et al.*, Pilot Study on Direct Ultrafiltration Treatment of High-Turbidity Seawater (China), *Ind. Water Treat.*, 2006, 20–23.
12 Y. H. Li, W. Zhang, X. J. Zhang, *et al.*, Experimental Study on Submerged Ultrafiltration Membrane Treatment of Slightly Polluted Surface Water in Rural Areas (China), *J. China Rural Water and Hydropower*, 2010, 50–53.
13 Z. Y. Jin, H. Gong and K. J. Wang, Application of hybrid coagulation microfiltration with air backflushing to direct sewage concentration for organic matter recovery, *J. Hazard. Mater.*, 2015, **283**, 824–831.
14 Z. Y. Jin, H. Gong, H. Temmink, *et al.*, Efficient Sewage Pre-concentration with combined coagulation microfiltration for organic matter recovery, *Chem. Eng. J.*, 2016, **292**, 130–138.
15 K. Kimura, D. Honoki and T. Sato, Effective physical cleaning and adequate membrane flux for direct membrane filtration (DMF) of municipal wastewater: Up-concentration of organic matter for efficient energy recovery, *Sep. Purif. Technol.*, 2017, **181**, 37–43.
16 P. Sanchis-Perucho, D. Aguado, J. Ferrer, *et al.*, Evaluating resource recovery potential and process feasibility of direct membrane ultrafiltration of municipal wastewater at demonstration scale, *Environ. Technol. Innov.*, 2023, **32**, 103252.
17 V. T. Kuberkar and R. H. Davis, Modeling of fouling reduction by secondary membranes, *J. Membr. Sci.*, 2000, **168**, 243–258.
18 N. Katagiri, T. Uchida, H. Takahashi and E. Iritani, An Evaluation of the Relationship between Membrane Properties and the Fouling Mechanism Based on a Blocking Filtration Model, *J. Separations*, 2024, **11**, 70.
19 B. Darwish, A. Alalawi, H. AlRomaih, N. Alotaibi and M. Aleid, Synthesis and performance of ultrafiltration membranes incorporated with different oxide nanomaterials: experiments and modeling, *J. Water Reuse*, 2023, **13**(3), 492–505.
20 Y. H. Li, *Membrane Fouling Characteristics of Submerged Ultrafiltration Membrane for Water Supply Treatment by Clay Particles and Organic Matter (China)*, D. Tsinghua University, 2011.
21 M. Qasim, A. Akbar, I. Khan, M. Ali, E. Lee and K. Lee, Evaluation of Organic and Inorganic Foulant Interaction Using Modified Fouling Models in Constant Flux Dead-End Operation with Microfiltration Membranes, *J. Membranes*, 2023, **13**, 853.
22 Y. M. Mei, *Study on the Efficiency and Optimization of Ultrafiltration Process for Emergency High-Turbidity Water Treatment (China)*, D. Harbin Institute of Technology, 2022.
23 H. Huang, T. A. Young and J. G. Jacangelo, Unified membrane fouling index for low pressure membrane filtration of natural waters: principles and methodology, *J. Environ. Sci. Technol.*, 2008, **42**, 714–720.
24 X. D. Kong, *Study on the Formation Mechanism and Application of Dynamic Membranes (China)*, D. Dalian University of Technology, 2015.
25 F. Zhang, G. Bournival, H. Ramandi and S. Ata, Digital Cake Analysis: A Novel Coal Filter Cake Examination Technique Using Microcomputed Tomography, *J. Minerals*, 2023, **13**(12), 1509.
26 X. Cheng, J. Lian, Z. Ren, C. Hou, Y. Jin, L. Zhang, X. Zhu, C. Luo, D. Wu and H. Liang, Coupling sodium percarbonate (SPC) oxidation and coagulation for membrane fouling mitigation in algae-laden water treatment, *Water Res.*, 2021, **204**, 117622.
27 G. Pereira, L. Cardozo-Filho, V. Jegatheesan and R. Guirardello, Generalization and Expansion of the Hermia Model for a Better Understanding of Membrane Fouling, *J. Membranes*, 2023, **13**(3), 290.
28 D. Gillett and A. Marchiori, A Low-Cost Continuous Turbidity Monitor, *J. Sens.*, 2019, **19**, 3039.

29 J. Trevathan, W. Read and S. Schmidtke, Towards the Development of an Affordable and Practical Light Attenuation Turbidity Sensor for Remote Near Real-Time Aquatic Monitoring, *J. Sens.*, 2020, **20**, 1993.
30 R. Bott, T. Langeloh and E. Ehrfeld, Dynamic cross flow filtration, *Chem. Eng. J.*, 2000, **80**, 245–249.
31 Q. Wang, X. Tang, H. Liang, W. Cheng, G. Li, Q. Zhang, J. Chen, K. Chen and J. Wang, Effects of Filtration Mode on the Performance of Gravity-Driven Membrane (GDM) Filtration: Cross-Flow Filtration and Dead-End Filtration, *J. Water*, 2022, **14**, 190.
32 M. Chun and W. Park, Time evolution of electrokinetic flow-induced streaming potential and flux in dead-end and cross-flow filtration of colloids through nanopores, *J. Membr. Sci.*, 2004, **243**, 417–424.
33 P. Romann, P. Giller, A. Sibilia, C. Herwig and A. Zydney, Co-current filtrate flow in TFF perfusion processes: Decoupling transmembrane pressure from crossflow to improve product sieving, *Biotechnol. Bioeng.*, 2023, **121**, 640–654.
34 S. Krishnan, B. Suzana, Z. Wahid, M. Nasrullah, M. Munaim, M. Fadhil, B. Din, S. Taib and Y. Li, Optimization of operating parameters for xylose reductase separation through ultrafiltration membrane using response surface methodology, *Biotechnol. Rep.*, 2020, **27**, e00498.
35 W. Park, S. Jeong, S. Im and A. Jang, High turbidity water treatment by ceramic microfiltration membrane: Fouling identification and process optimization, *Environ. Technol. Innov.*, 2020, **17**, 100578.
36 T. Mattsson, W. Lewis, Y. Chew and M. Bird, The use of fluid dynamic gauging in investigating the thickness and cohesive strength of cake fouling layers formed during cross-flow microfiltration, *Sep. Purif. Technol.*, 2018, **198**, 25–30.
37 E. Iritani and N. Katagiri, Developments of Blocking Filtration Model in Membrane Filtration, *Kona Powder Part. J.*, 2016, **33**, 179–202.
38 M. Vela, S. Blanco, J. García and E. Rodríguez, Analysis of membrane pore blocking models applied to the ultrafiltration of PEG, *Sep. Purif. Technol.*, 2008, **62**, 489–498.
39 E. Iritani, N. Katagiri, Y. Ishikawa and D. Cao, Cake formation and particle rejection in microfiltration of binary mixtures of particles with two different sizes, *Sep. Purif. Technol.*, 2014, **123**, 214–220.
40 M. Hennemann, M. Gastla and T. Beckera, Optical method for porosity determination to prove the stamp effect in filter cakes, *J. Food Eng.*, 2021, **293**, 110405.